



OTC 12102

Optimization of Reservoir Simulation and Petrophysical Characterization in 4D Seismic

Gilles Guerin, Wei He, Roger N. Anderson and Liqing Xu, Lamont-Doherty Earth Observatory, and Ulisses T. Mello, IBM Watson

Copyright 2000, Offshore Technology Conference

This paper was prepared for presentation at the 2000 Offshore Technology Conference held in Houston, Texas, 1-4 May 2000.

This paper was selected for presentation by the OTC Program Committee following review of information contained in an abstract submitted by the author(s). Contents of the paper, as presented, have not been reviewed by the Offshore Technology Conference and are subject to correction by the author(s). The material, as presented, does not necessarily reflect any position of the Offshore Technology Conference or its officers. Electronic reproduction, distribution, or storage of any part of this paper for commercial purposes without the written consent of the Offshore Technology Conference is prohibited. Permission to reproduce in print is restricted to an abstract of not more than 300 words; illustrations may not be copied. The abstract must contain conspicuous acknowledgment of where and by whom the paper was presented.

Abstract

4D seismic has become a widely accepted technique to interpret changes between successive 3D seismic surveys in terms of fluid substitution and pressure depletion in a producing reservoir. However, most time-lapse studies have been mostly qualitative and based on simplified reservoir representation in order to adjust to the time constraints of today's oil market.

In this paper, we present how reservoir simulation constrained by stochastic characterization and non-linear optimization can be used in an integrated series of tools to refine 4D interpretation.

Because of its direct relationship with pore fluid content and properties, we use seismic impedance rather than seismic amplitude as the primary data between the various steps of our 4D interpretation loop. Non-linear inversion of the 3D seismic data sets allows a preliminary interpretation. Stochastic simulation of the lithology and porosity, constrained by these "observed" impedance volumes and by well logs, provide the static reservoir characterization for the reservoir simulator. Once simulated production matches the recorded production history, empirical or Biot/Gassmann-type petrophysical models are used to calculate the "simulated" impedance volume from the fluid saturation and pressure distribution calculated by the reservoir simulator. Non-linear optimization is used iteratively to improve first the production history match and next the agreement between "simulated" and "observed" impedance volumes over time. This optimization is performed over a limited set of poorly constrained parameters in the permeability calculation and petrophysical models. In the case study presented here, the analysis of a turbidite reservoir in the South Timbalier 295 field, our results show

how stochastic characterization helps reproducing the complexity of reservoir fluid dynamics while the results of the optimization underlines the robustness of the 4D interpretation despite the large amount of unknowns.

Introduction

Time-lapse, or 4-D, seismic monitoring is an integrated reservoir exploitation technique based on the analysis of successive 3D seismic surveys. Differences over time in seismic attributes are directly related to changes in pore fluids and pore pressure during the drainage of a reservoir under production. The detection of areas with significant changes or with unaltered hydrocarbon-indicative attributes, can be used to determine drilling targets where hydrocarbons remain trapped after several years of production. Making sure that seismic differences are related to fluid flows is critical for a complete time-lapse seismic study. Noise associated with differences in acquisition can generate seismic differences between surveys that are not related to the reservoir drainage pattern.

In this paper, we describe how reservoir simulation can be used to generate independent impedance maps to validate or constrain 4-D impedance maps obtained from the inversion of successive legacy data sets. A complete 4D analysis is an iterative loop where the original interpretation can be refined along the later steps. First, we summarize the steps preceding the reservoir simulation, including the 3D seismic processing and inversion, and the preliminary time-lapse interpretation. We then describe the elastic models, the properties of reservoir fluids and the reservoir characterization that can be used to link the impedance volumes to fluid and lithology distributions in the reservoir. The results of the simulation are finally used to generate impedance maps that can be compared with seismic inversion results. Because of the large number of poorly constrained parameters used to describe complex reservoirs, the different steps of the interpretation have to be optimized to match at best simulation results and observations. The first optimization loop is applied to the reproduction of the production history by the simulator, using parameters such as relative permeability or aquifer support. The second stage of optimization is in deriving impedance maps from simulated saturation, which involves the choice of an elastic formulation

and the reservoir fluid properties. To illustrate the different steps of the entire procedure we use the case study of the K8 reservoir, South Timbalier 295, offshore Louisiana.

The 4D seismic loop:

Non linear inversion of successive 3D datasets

Since its emergence, time-lapse analysis has been usually applied to changes in seismic amplitudes. However, amplitudes are only proportional to seismic reflectivity, which depends on the relative variability in the elastic properties of the formation, not on the value of these properties.

In contrast, seismic impedance, the product of density (ρ) and compressional velocity (V_p) is directly related to the elastic properties of the sediments. ρ is the volumetric average of the density of the different phases (fluids and solids) and V_p can be explicitly expressed as a function of their density and compressibility. Also, unlike amplitudes, a simple algebraic subtraction between the impedance volumes at two dates can be directly converted into fluid or pressure changes. Therefore a 4D analysis based on impedance volumes instead of amplitudes allows a direct qualitative interpretation of seismic changes in terms of fluid substitution or migrations. We use a constrained non-linear inversion technique to estimate the acoustic impedance volumes from each 3D survey¹.

Preliminary 4D interpretation of the K8 sand

The K8 reservoir in the South Timbalier 295 field, offshore Louisiana (**Fig. 1**). It produced about 350,000 m³ of oil and 150 millions m³ of gas between two 3D surveys shot in 1989 and 1994. The K8 sand is a complex combination of channelled mid-fan sheet sands lapping on a paleo-high in the east and gently dipping to the South West (**Fig. 2**). **Fig.3** shows the results of the inversion of the two surveys shot in 1989 and 1994 over K8. The difference between the two inversions (**Fig. 3c**) shows a global decrease in impedance (red) in most of the shallower layers and updip (NE) from the two producing wells in the deeper layers. Impedance has mostly increased (blue) in the deeper layer of the reservoir between the two surveys. Because the reservoir was originally filled with oil, and the replacement of oil by gas or water respectively decreases or increases the density and the sonic velocity of the formation, oil might have been replaced mostly by gas in the shallower layers of the reservoir and by water in the deeper layers. The substitution of oil by gas exsolution updip is controlled by the pressure decrease induced by the producing wells while the replacement of oil by water in the deeper layers is assisted by the presence of an aquifer supporting the reservoir².

Independently of the nature of the pore fluid, the bulk of the impedance of such medium porosity sediments (40% maximum) is mostly controlled by the porosity and lithology distributions. To relate quantitatively the observed changes in impedance with the nature and the volume of the pore fluids, it is necessary to have a complete representation of the sediment matrix, and to define the relationships between the different components of the system and its elastic properties.

Petrophysical characterization of reservoirs

Elastic models. Explicit relationships relating pressure, pore fluid, porosity, matrix materials and the elastic properties of marine sediments have been the topic of various theoretical^{3,4} or empirical^{5,6} studies. They are all limited in application by the infinite number of parameters affecting the elastic properties of sediments and no approach can offer a comprehensive formulation. We review in the Appendix some commonly accepted models and relationships that could be used to link the changes observed in our impedance maps with changes observed in the reservoirs.

Fluid properties. For any of these elastic models, the changes observed in impedance over time will depend on the elastic properties of the pore fluid, which are the primary parameters responsible for changes in impedance during production.

Properties of fluid mixtures. The properties of the pore fluid that affect the elastic properties of a reservoir are in fact the properties of a fluid mixture, which is a function of the properties of the various fluid phases. The three primary types of pore fluid in a reservoir are hydrocarbon gas (gas) hydrocarbon liquid (oil), and brine. The density (ρ_f) and the compressibility ($1/K_f$) of the mixture are respectively the weighted averages of the density and of the compressibility of the three phases

Elastic properties of reservoir fluids. Physical properties of reservoir fluids are dependant on composition, pressure and temperature⁷. Unless thermal recovery techniques are used, the variations of temperature in a reservoir are negligible during its production history, and pressure and composition are the dominant parameters affecting the changes observed between two surveys. In addition to the relationships defined in the literature⁷, we also use simple linear relationships between pressure and elastic properties in our optimization, based on available laboratory data (Gas and oil gravities, reservoir Gas Oil Ratio) and a few rules: density and velocity of gas and brine decrease with decreasing reservoir pressure, velocity and density of oil decrease with decreasing pressure while pressure is above bubble point, and increase below bubble point as lighter component come out of solution

Stochastic reservoir characterization. The final link between impedance volumes, fluids properties, saturations and pressure distribution resides in the characterization of the reservoir porosity and lithology distribution. We use geostatistical simulations for this characterization, assuming that within an individual reservoir petrophysical and acoustic properties are closely related and can be associated with calibrated cross-correlation functions¹. Sixteen wells provided the hard data used to constrain the reservoir characterization of K8 (**Fig. 4**). Both porosity and shale distributions show a high level of heterogeneity, illustrating the channelled deposition of the reservoir. The bulk of the porosity is located immediately

down dip from the two producing wells and in the South East corner of the study area.

From saturations to impedances. The completed characterization of fluid and reservoir characterization properties allows to use any of the petrophysical models to calculate the impedance volumes when pressure and fluid distributions are known, such as before the beginning of production in 1988, when oil/gas and oil/water contacts can be assumed horizontal. In Fig. 5, the crossplots of the different models with the 1988 impedance allow to compare their respective validity. In all these figure, a perfect formulation should result in an identical linear fit with the inverted values. The KT and Gassman+KT impedances (Figs 5a and 5b) display the highest level of scattering and consequently the poorest agreement with the inversion results. The Han and Gassmann+Han impedances present the best agreement with the inversion, with regression coefficients higher than 0.80. It is necessary, however, to make a similar comparison after simulation to evaluate how fluid substitution affects the comparison between the calculated and the inverted impedance.

Comparison with vertical sweep. This preliminary validation of the elastic formulations can be used to illustrate the need for an accurate understanding of the reservoir dynamics that time-lapse seismic can provide. A traditional view of the fluid movements within a producing reservoir is of a uniform buoyancy-driven movement of the different phases, the contact surfaces between adjacent phases remaining horizontal. Assuming that the GOC and WOC have been simply sweeping uniformly along dip, and that the reservoir is still globally in hydrostatic equilibrium at any time, we have calculated the pressure and fluid distribution that would exist in 1994 if an horizontal gas cap had formed down to 3280 mbsf and the WOC had moved up to 3320 mbsf. The impedances calculated from these values using the Gassmann+Han formulation are shown in Fig. 6. Comparison with Fig. 3 shows that the impedances calculated present strong similarities with the 1994 inversion results. The impedance changes over time (Figures 3.4c and 3.8c) also display some global similarities: decrease in impedance updip from the wells, and increase downdip. However, the pattern and the absolute values of the observed impedance changes are much more heterogeneous in Fig 3c than in this simple ‘gravitational sweep’. The bright areas in the observed impedance changes correspond to isolated impedance decreases, that could indicate areas with low connectivity where hydrocarbon, mostly gas, would remain trapped as the reservoir pressure decreases. The comparison of Figs 3.4c and 3.8c shows that after a few years of intense production, the representation of a GOC as a continuous horizontal surface is merely irrelevant. The fact that the impedances calculated after the reservoir sweep compare reasonably well with the inversion results in 1994, despite the major differences in the changes over time (Fig. 3c vs. Fig 6c), shows how crucial it is for each inversion to be the most accurate, as differentiating

between the inversions of successive surveys is much more sensitive to errors than either inversion.

Reservoir Simulation

The entrapment of hydrocarbons is mostly the result of the heterogeneity in the reservoir and in the permeability distribution. Assuming that our inversion results are correct, the heterogeneity observed in the impedance difference over time suggests a migration process more complex than the simple gravitationnal sweep. Numerical simulation of the migration of the different phases can be used to identify the actual behavior of the reservoir under production.

Permeability distribution. In addition to porosity, the primary control on the reservoir drainage is the permeability distribution. While permeability is directly related to porosity, it can also be affected considerably by the presence of shales. The effective permeability of shaly sandstones can be calculated from porosity and shale fraction (γ) by:

$$k = k_{ss} \cdot (1 - \gamma)^m = \alpha \exp(\beta \Phi) \cdot (1 - \gamma)^m \dots \dots \dots (1)$$

where m is an exponent dependant on the aspect ratio of the clay minerals⁸. α and β can be measured on clean sand samples. The permeability distribution in K8 is shown in Fig. 7.

Multiple-phase fluid flows in porous media. Reservoir simulation is based on solving the mass conservation equation of multiple-phase fluids in porous media, using Darcy’s law for multi-phase fluid flows in porous media:

$$\vec{q} = -k \cdot \sum_{\phi=o,g,w} S_{\phi} \rho_{\phi} \frac{k_{r\phi}}{\mu_{\phi}} [\vec{\nabla} P_{\phi} - \rho_{\phi} \vec{g}] \dots \dots \dots (2)$$

where q is the three-phase fluid velocity, the subscript ϕ refers to the attributes of each phase: saturation (S), pressure (P), density (ρ_{ϕ}), viscosity (μ_{ϕ}) and relative permeability (k_r). k is the absolute permeability of the formation and \vec{g} the gravity acceleration.

The relative permeability of each phase (oil, water, gas) increases with its saturation and can be calculated in three phases fluid as a combination of the relative permeabilities of two-phases fluid mixtures:

$$k_{ro} = \frac{S_g k_{rog} + (S_w - S_{wco}) k_{row}}{S_g + S_w - S_{wco}} \dots \dots \dots (3)$$

where k_{rog} and k_{row} are the oil relative permeability for systems with oil and gas only and oil and water only, respectively. S_{wco} is the connate, or irreducible, water saturation. The variations of k_{rg} and k_{rog} , as a function of gas saturation and of k_{rw} and k_{row} as a function of water saturation, called saturation functions, are rarely available. No relative permeability measurements were available for K8 and since this absence has to be expected in most reservoir, relative permeabilities are one of the adjustable parameters within the optimization of the production history match.

Simulator description. The code used to solve Eq (2) is ECLIPSE, a commercial three phase, three dimensional finite

differences simulator using a corner point geometry grid that allows to define highly distorted nodes to represent the reservoir geometry⁹.

Since the only actual measurable effects of the reservoir drainage are the volumes of hydrocarbons collected at the surface, the production history recorded on the rig floor is the principal constraint on the simulator. It is expressed in terms of daily production rate of oil or gas for each well, and averaged monthly. This imposed production is translated into pressure gradients between the wellbores and the formation, which are echoed in the reservoir at each time step of the simulation.

In addition to the perforated well intervals the only flows allowed in and out the reservoir model are from eventual aquifers, in order to simulate possible aquifer support. The strength of this support is defined in water influx per unit pressure difference. All other model boundaries are considered impermeable, either lithologically (shaded out) or structurally (sealing faults).

Simulation results

History match. Fig. 8 shows how the simulator was able to reproduce the production history of K8, starting from the initial conditions in 1988. Dots represent observed production data and the lines the simulation results. Because oil production was the imposed control mechanism, the perfect match for this production is expected. The optimization of the production history was done on two parameters: the exponent in the gas relative permeability, and the location of the aquifer support, whether from the west, or directly underneath the reservoir. The comparison of the different figures shows that the best match in the gas and pressure histories are with a 0.9 exponent in gas relative permeability and an aquifer support underneath the reservoir.

Even without matching the exact production history, the simulation helps to understand the dynamics in the reservoir. Fig. 9 shows the simulated oil and gas streamlines in May 1993, while the two wells are producing at their peak. The differences between the various figures, and the differences in production matching results show how reservoir simulation success can be sensitive to a limited number of poorly constrained parameters.

Fluid saturations and impedance. The oil and gas distributions at the end of the simulation (Fig. 10) have to be compared with the uniform values of 70% oil and no gas at the origin of the simulation. Fig. 11 shows the impedance volumes and change over time calculated with these values using the Gassmann+Han formulation. The simulated impedance distribution in 1994 seems very similar to the inversion results at this date (Fig 3b), but to confirm that this relationship still offers the best representation of the reservoir properties after fluid substitutions, we also calculated the impedances after the simulation with the other petrophysical formulations. A similar crossplot analysis as conducted in 1988 shows that the Gassmann+Han models still presents the best comparison with the inverted impedance after fluid

substitutions.

End of the 4D loop

Improving the present results and, more generally, the optimization of the 4D interpretation loop can take several forms. We have developed a procedure to automatically optimize the production history and the impedance maps, after identifying various numerical parameters and 'loose' reservoir properties. These procedures can be applied automatically to such parameters as grain or frame moduli, fluid properties or empirical parameters in the experimental relationships described in the appendix.

Recurrently missing properties and numerical parameters such as relative permeability functions, critical saturations, capillary pressures, aquifer strength or permeability factors can be varied between successive simulations in order to find a better history match. Upscaling the reservoir model dimensions for shorter computation times, it is possible to automate the variation of some of these arbitrary numerical parameters or loosely constrained properties to minimize the difference between measured and simulated production history.

To complete the loop, the impedance volumes calculated from the reservoir simulation results have to be fed into a 3D seismic waves propagation elastic model to try to reproduce the observed datasets. For this purpose, we have built tools allowing to remesh the simulation grid within the original data volume¹⁰ and developed a full elastic 3D finite difference model to simulate the propagation of seismic waves and generate a synthetic seismic amplitude volume. The comparison of the simulated amplitudes with the original datasets can be used as a simple validation of the reservoir simulation, but it can also be used to re-evaluate the inversion or the reservoir characterization results when data are missing or unreliable.

Conclusions

These are mere possibilities for the 4D interpretation to proceed from reservoir simulation to get an exact understanding of the reservoir dynamics. Because the exploration, production history and the configuration of each reservoir are unique, there is no exhaustive procedure for time-lapse monitoring. We have tried to develop an integrated series of tools allowing to apply our general methodology to any reservoir, but its flexibility requires a clear understanding of the possible sources of errors in order to use the iterative procedure to minimize them.

At the junction between complex theoretical methods (non-linear seismic inversion, 3D elastic modelling or stochastic simulation) and the most primary field data, reservoir simulation provides the link between the observed changes in seismic attributes, the hydrocarbons produced on the rig floor and the actual fluid dynamics within a reservoir. Because it should ultimately indicate where to drill to recover trapped hydrocarbon, and the volumes to expect, it can help understand the passed history of a reservoir, but more importantly, how to make the best of its future. In the case of

the K8 sand, the good agreement between simulation and inversion indicate that the final optimization should be only a refinement of the present results.

References:

1. He, W., 1996, 4-D Seismic Analysis and Geopressure Prediction in the Offshore Louisiana, Gulf of Mexico. Ph.D. Thesis, Columbia University.
2. Mason, E.P., 1992, Reservoir geology and production performance of turbidite sands at South Timbalier 295 field, offshore Louisiana, in transactions of the Gulf Coast Association of Geological Societies, Vol XLII, 267-278.
3. Gassmann, F., 1951, Elastic waves through a packing of spheres, *Geophysics*, 16, 673-685.
4. Kuster, G.T., and M.N. Toksöz, 1974, Velocity and attenuation of seismic waves in two-phase media, 1, Theoretical formulation, *Geophysics*, 39, 587-606.
5. Han, D-H., A. Nur and D. Morgan, 1986, Effects of porosity and clay content on wave velocities in sandstones, *Geophysics*, 51(11), 2093-2107.
6. Ramamoorthy, R., W.F. Murphy and C. Croll, 1995, Total porosity estimation in shaly sands from shear modulus, Trans. SPWLA 36th Logging Symposium, paper H.
7. Batzle, M., and Z. Wang, 1992, Seismic properties of pore fluids, *Geophysics*, 57(11):1396-1408.
8. McCarthy, J.F., 1991, Analytical models of the effective permeability of sand-shale reservoirs, *Geophys. J. Int.*, 105, 513-527.
9. Ponting, D.K., 1989, Corner Point Geometry in Reservoir Simulation, proc. Joint IMA/SPE European Conference on the Mathematics of Oil Recovery, Cambridge.
10. Mello, U.T., P.R. Cavalcanti, A. Moraes and A. Bender, 1998, New developments in the 3D simulation of evolving petroleum systems with complex geological structures, AAPG international conference and exhibition abstracts, AAPG Bulletin, 82(10), p. 1942.
11. Hamilton, E. L., 1971, Elastic properties of marine sediments, *J. Geophys. Res.*, 76, 579-601.
12. Hamilton, E. L., Bachman, R. T., Berger, W. H., Johnson, T. C., and Mayer, L. A., 1982, Acoustic and related properties of Calcareous deep-sea sediments, *J. Sed. Pet.*, 52(3), 733-753.
13. Guerin, G., and D. Goldberg, 1996, Acoustic and elastic properties of calcareous sediments across a siliceous diagenetic front on the eastern U.S. continental slope, *Geophys. Res. Lett.*, 23(19), 2697-2700.

Appendix - Elastic models for sediments properties

Most models define relationships for the elastic moduli of the formation instead of the impedance. The bulk modulus (K) is the inverse of its compressibility and the shear modulus (G) a measure of its shear strength. Compressional and shear (V_s) sonic velocity can be expressed as functions of these moduli and of the density of the sediments:

$$V_p = \sqrt{\frac{1}{\rho} \left(K + \frac{4}{3} G \right)} \dots\dots\dots(A-1)$$

and $V_s = \sqrt{\frac{G}{\rho}} \dots\dots\dots(A-2)$

and the impedance (Z) can simply be re-written

$$Z = \rho V_p = \sqrt{\rho \left(K + \frac{4}{3} G \right)} = \sqrt{\rho K + \frac{4}{3} \rho^2 V_s^2} \dots\dots\dots(A-3)$$

Theoretical formulations. Gassmann (1951) expressed the bulk modulus of fluid-saturated sediments as a function of the bulk moduli of the dry frame (K_f), of the pore fluid (K_f) and of the grains (K_g)

$$K = K_g \frac{K_f + Q}{K_g + Q} \text{ with } Q = \frac{K_w (K_g - K_f)}{\Phi (K_g - K_w)} \dots\dots\dots(A-4)$$

Empirical relationships for K_f as a function of porosity have been established for several types of lithology^{11,12}. Using his results for clay, silts and fine sands, we use a single formula for clastic sediments:

$$\log(K_f) = \log(K_g) - 4.25\Phi \text{ or } \log(K_f/K_g) = -4.25\Phi \dots\dots(A-5)$$

The grain modulus of a shale/sand mixture can be calculated by a Voigt-Reuss-Hill average of the grain moduli of sand (K_s) and clay (K_c)¹¹:

$$K_g = \frac{1}{2} \left[\gamma K_c + (1 - \gamma) K_s + \frac{K_s K_c}{K_s \gamma + K_c (1 - \gamma)} \right] \dots\dots\dots(A-6)$$

where γ is the shaliness or volumetric shale fraction. We refer to it as the Gassmann/Hamilton model¹³.

The theory of sonic waves scattering and propagation has also been used to calculate the effective elastic moduli of a two phase medium made of spherical inclusions in a uniform matrix⁴:

$$K = K_m \frac{1 + [4G_m (K_i - K_m) / ((3K_i + 4G_m) K_m)] I_c}{1 - [3(K_i - K_m) / (3K_i + 4G_m)] I_c} \dots\dots\dots(A-7)$$

and

$$G = G_m \frac{(6K_m + 12G_m) G_i + (9K_m + 8G_m) [(1 - I_c) G_m + I_c G_i]}{(9K_m + 8G_m) G_m + (6K_m + 12G_m) [(1 - I_c) G_i + I_c G_m]} \dots\dots\dots(A-8)$$

where the i and m subscripts refer to the inclusion and the matrix properties, respectively, and I_c is the volumetric fraction of the inclusion.

Experimental relationships. Underlining the practical limits of these theoretical relationships, the following linear relationships have been established between ultrasonic velocities, porosity and clay content⁵:

$$V_p = 5.59 - 6.93\Phi - 2.18\gamma \dots\dots\dots(A-9)$$

$$V_s = 3.52 - 4.91\Phi - 1.89\gamma \dots\dots\dots(A-10)$$

Using *in situ* data from shear sonic geochemical logs the following relationship has been drawn for the shear modulus of shaly sediments⁶:

$$G = G_{\text{grain}} (1 - 3.48\Phi + 2.19\Phi^2) \dots\dots\dots(A-11)$$

$$\text{With } G_{\text{grain}} = (0.039 \log_{10}(_) + 0.072)^{-1} \dots\dots\dots(A-12)$$

G_{grain} is the effective grain shear modulus.

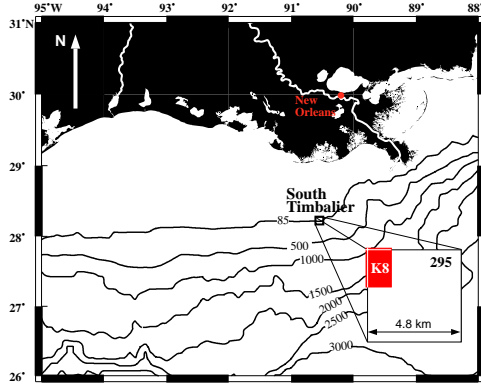


Figure 1 Location map of the K8 field, South Timbalier Block 295. The grey areas shows the actual overlap between successive surveys that were used in the 4D analysis.

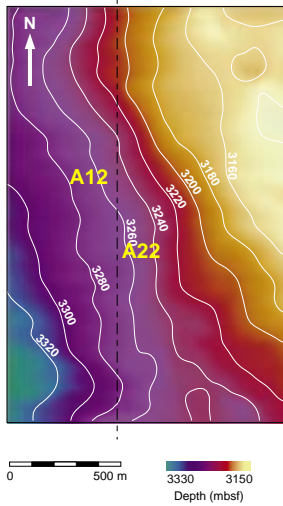


Figure 2 Structure of the top of the K8 reservoir. The reservoir dips slightly to the South West and leans on a paleohigh to the east. A12 and A22 are the two wells producing between the 1988 and 1994 surveys

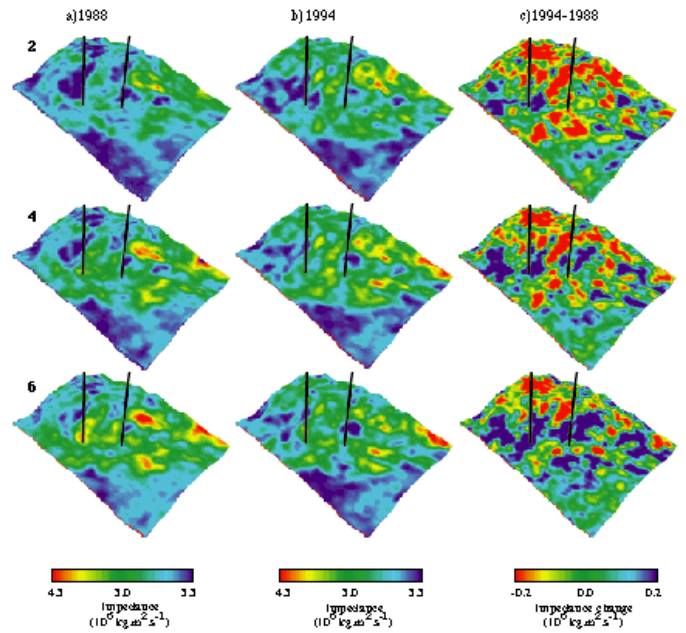


Figure 3: Results of the impedance inversion of 3D seismic surveys of K8 in 1988 (a) and 1994 (b). The layers are numbered from bottom to top. By convention, for consistency with the seismic 'brightening' usually associated with free gas, low impedance values are in red and high impedance in blue. (c) Difference between the two impedance inversions. Impedance decrease between 1988 and 1994 is in red. The two producing wells are indicated by the black lines.

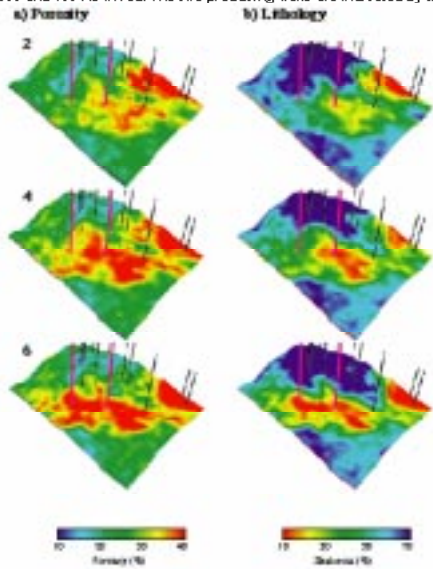


Figure 4. Results of the stochastic reservoir characterization of K8: (a) porosity (b) shaliness. For visual coherence between the two figures, high shaliness (low sand content and low porosity) is in blue. In addition to the two producing wells (shown in red), the other wells used for the calibration of the reservoir characterization are shown (black).

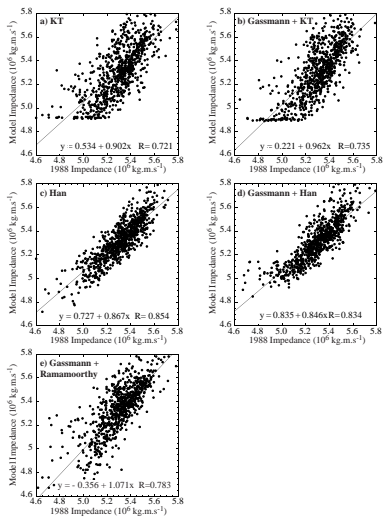


Figure 5: Comparison of the predictions of the various petrophysic models with the impedance inversion of 1988, before production. (a) KT, (b) Gassmann+KT, (c) Han, (d) Gassmann+Han and (e) Gassmann+Ramamoorthy. Equations of the linear fits and regression coefficients (R) are given in each figure.

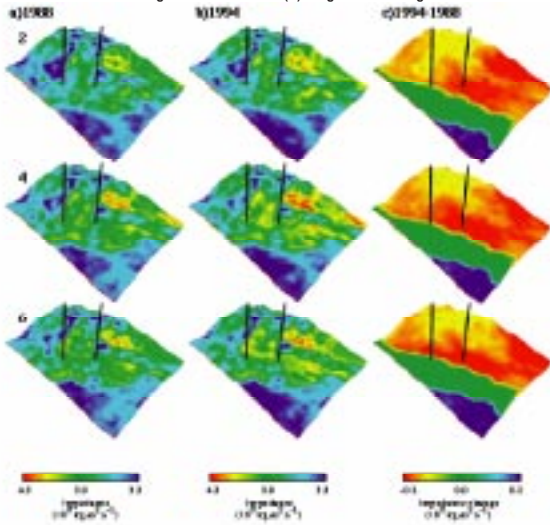


Figure 6: Evolution of the reservoir impedance distribution in the case of a uniform sweep of the reservoir. (a) Impedance calculated before production, when the reservoir fluids are in hydrostatic equilibrium. Oil saturation is uniformly 70%, the rest of the pore space corresponds to connate water. (b) Impedance distribution if the gas cap had migrated uniformly down to 9200 about between 1989 and 1994. (c) Change in impedance that would be observed in this simple case.

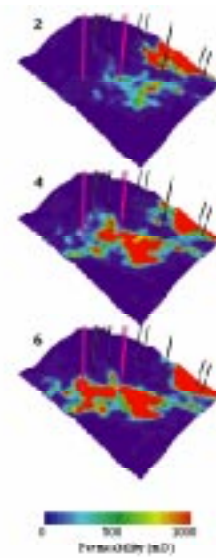


Figure 7: Permeability distribution in K0, calculated from the results of the reservoir characterization and the permeability/porosity relationship derived from K0 core samples. All the wells used for the reservoir characterization are shown.

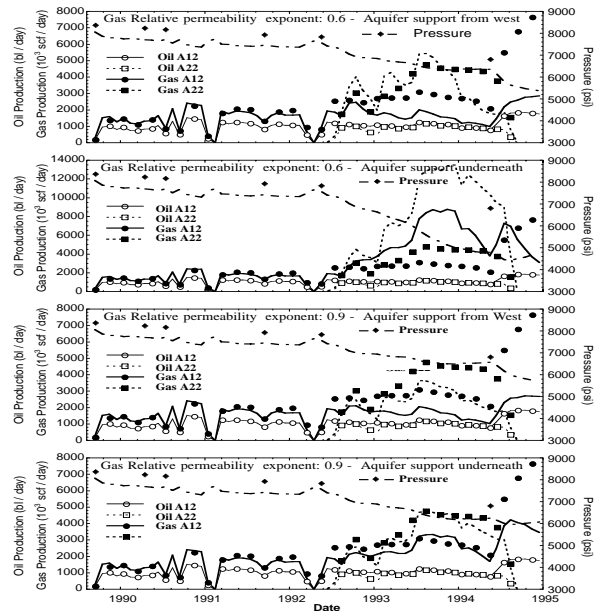


Figure 8: Production history match for different reservoir configurations - the optimizing procedure is applied to the gas relative permeability exponent and to the aquifer position. In all figures, discrete symbols (square and circle) represent measured data and lines represent simulation results.

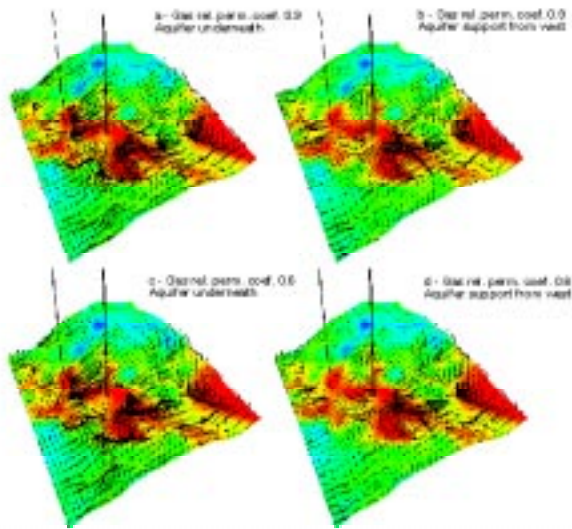


Figure 9: Simulated oil streamlines for different values of exponent in gas relative permeability and in the configuration of the aquifer support.

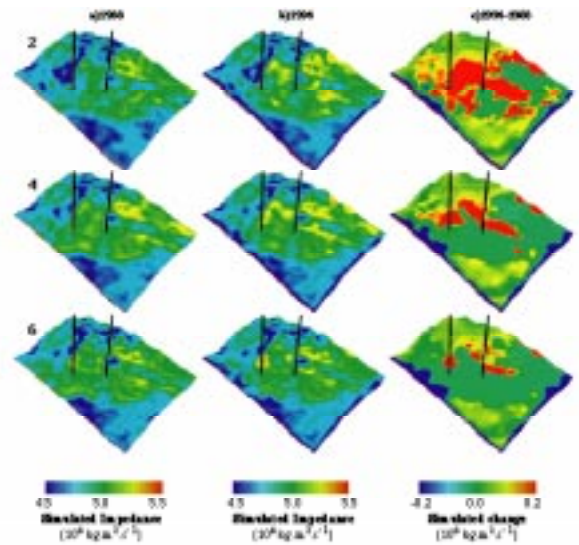


Figure 11: Impedances calculated from the simulation results in N6 in 1996 (a), and in 1994 (b). (c) Difference between the two time steps.

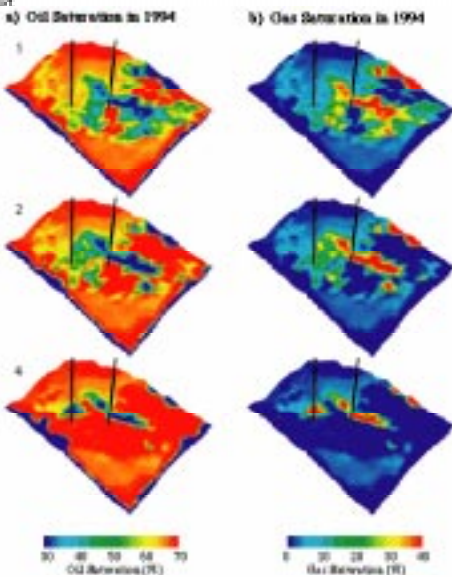


Figure 10: (a) Oil and (b) gas saturation at the end of the simulation of N6. At the beginning of the simulation, they were uniformly 70% and 0%, respectively.